

Implementation of the HMC algorithm on the tempered Lefschetz thimble method

Masafumi Fukuma^{1*}, Nobuyuki Matsumoto^{1†} and Naoya Umeda^{2‡}

¹*Department of Physics, Kyoto University, Kyoto 606-8502, Japan*

²*PricewaterhouseCoopers Aarata LLC,
Otemachi Park Building, 1-1-1 Otemachi, Chiyoda-ku, Tokyo 100-0004, Japan*

Abstract

The tempered Lefschetz thimble method (TLTM) is a parallel-tempering algorithm towards solving the numerical sign problem, where the system is tempered by the antiholomorphic gradient flow to tame both the sign and ergodicity problems simultaneously. In this paper, we implement the hybrid Monte Carlo (HMC) algorithm for transitions on each flowed surface, expecting that this implementation on TLTM will give a useful framework for future computations of large-scale systems including fermions. Although the use of HMC in Lefschetz thimble methods has been proposed so far, our crucial achievement here is that HMC is implemented on TLTM so as to work within the parallel-tempering algorithm in TLTM, especially by developing an algorithm to handle zeros of fermion determinants in the course of the molecular-dynamics process. We confirm that the algorithm works correctly by applying it to the sign problem of the Hubbard model on a small lattice, for which the TLTM is known to work with the Metropolis algorithm. We show that the use of HMC significantly reduces the autocorrelation times with less computational times compared to the Metropolis algorithm.

*E-mail address: fukuma@gauge.scphys.kyoto-u.ac.jp

†E-mail address: nobu.m@gauge.scphys.kyoto-u.ac.jp

‡E-mail address: naoya.umeda1134@gmail.com

Contents

1	Introduction	1
2	Preparations	3
2.1	Tempered Lefschetz thimble method (review)	3
2.2	Real representation for complex variables	5
2.3	Outline for the implementation of HMC on TLTM	6
3	Molecular dynamics on flowed surfaces	7
3.1	Molecular dynamics on a general constrained surface	7
3.2	Molecular dynamics on a flowed surface Σ_t	10
4	HMC on TLTM	15
4.1	Swap of configurations at adjacent replicas	15
4.2	Summary of HMC on TLTM	17
5	Results and analysis	19
5.1	Hubbard model and the parameters for simulations	19
5.2	Estimate of the number density	21
5.3	Autocorrelations	23
6	Conclusion and outlook	25
A	More on the treatment of zeros	27

1. Introduction

The Markov chain Monte Carlo (MCMC) method has been an important tool in theoretical physics as it enables nonperturbative calculations of physical quantities. However, its application to some important research areas is still hindered due to the numerical sign problem. Examples include finite density QCD [1], the quantum Monte Carlo simulations of strongly correlated electron systems [2, 3], and real-time quantum field theories. Among many approaches towards solving the sign problem, algorithms using Lefschetz thimbles [4, 5, 6, 7, 8, 9, 10, 11, 12] have been developed because of its mathematical rigor [13]. Along the line of such developments, the *tempered Lefschetz thimble method* (TLTM) was

proposed [11, 12] as a versatile solution to the sign problem.¹

As will be reviewed in the next section, the TLTM is a parallel-tempering algorithm, where the tempering parameter is set to be the flow time of the antiholomorphic gradient flow. This is to resolve the dilemma between the sign and ergodicity problems that becomes manifest when contributions from multiple thimbles are relevant. The validity of TLTM has been confirmed for various models, including the $(0+1)$ -dimensional massive Thirring model [11], the Hubbard model away from half filling [12] and a class of chiral matrix models (to be reported in another communication).

As an algorithm to generate transitions on each flowed surface in TLTM, we have adopted the Metropolis algorithm in our previous study because of its simplicity. However, it is known that the Metropolis algorithm becomes less efficient than the Hybrid Monte Carlo (HMC) algorithm for systems including fermions with large degrees of freedom [15, 16]. Thus, the implementation of HMC on TLTM must give a useful framework for future computations of large-scale systems including fermions.

Our implementation of HMC on TLTM is based on the RATTLE algorithm [17, 18] to realize molecular dynamics on flowed surfaces. RATTLE was first introduced to Lefschetz thimble methods in [7] for molecular dynamics on a single Lefschetz thimble, and was generalized in [19] for that on a flowed surface at finite flow time. Our achievement here is that HMC is implemented on TLTM so as to work within the parallel-tempering algorithm in TLTM, especially by developing an algorithm to handle zeros of fermion determinants in the course of the molecular-dynamics process.² To demonstrate that the implementation works correctly with high efficiency, we apply it to the Hubbard model away from half filling with small degrees of freedom ($N = 20$ for an $N_s = 2 \times 2$ spatial lattice with $N_\tau = 5$ imaginary time steps), for which the TLTM is known to work correctly with the Metropolis algorithm [12].³ We show that our new algorithm gives results that agree nicely with exact values, and the computational cost to obtain an independent configuration is reduced to about 30% of that of the Metropolis algorithm. We expect that greater efficiency will be gained for larger degrees of freedom.

This paper is organized as follows. In section 2, we first review the basics of TLTM. Then, after a short explanation on our convention, we give an outline for the implementation of HMC on TLTM. We in section 3 explain a general theory for molecular dynamics on flowed surfaces, and in section 4 give an explicit algorithm to implement HMC on TLTM. The algorithm is applied to the Hubbard model in section 5, and is shown to work correctly with

¹See [14] for a similar idea.

²Handling zeros of fermion determinants (in complex space \mathbb{C}^N) is necessary because they are reached with finite flow times and configurations around them can be relevant to observables under consideration.

³See [20, 21, 22, 23] for related work on the application of Lefschetz thimble methods to the Hubbard model.

reduced computational costs compared with the Metropolis algorithm. Section 6 is devoted to conclusion and outlook.

2. Preparations

In this section, we first review the basics of TLTM. Then, after a short explanation on our convention, we give an outline for the implementation of HMC on TLTM.

2.1. Tempered Lefschetz thimble method (review)

Let $\mathbb{R}^N = \{x\}$ be a configuration space of N -dimensional real variable $x = (x^i)$ ($i = 1, \dots, N$), and $S(x)$ the action. Our main concern is to estimate the expectation value of an observable $\mathcal{O}(x)$,

$$\langle \mathcal{O}(x) \rangle \equiv \frac{\int_{\mathbb{R}^N} dx e^{-S(x)} \mathcal{O}(x)}{\int_{\mathbb{R}^N} dx e^{-S(x)}}. \quad (2.1)$$

In this paper, we always assume that both $e^{-S(z)}$ and $e^{-S(z)} \mathcal{O}(z)$ are entire functions over \mathbb{C}^N .⁴ Then, due to Cauchy's theorem in higher dimensions, the integrals in (2.1) do not change under continuous deformations of the integration region from \mathbb{R}^N to Σ with the boundary at $|x| \rightarrow \infty$ kept fixed:

$$\langle \mathcal{O}(x) \rangle = \frac{\int_{\Sigma} dz e^{-S(z)} \mathcal{O}(z)}{\int_{\Sigma} dz e^{-S(z)}}. \quad (2.2)$$

The sign problem will then get much reduced if $\text{Im } S(z)$ is almost constant on Σ .

The Markov chain Monte Carlo (MCMC) calculation of (2.2) can be performed as follows. First, we decompose the complex measure $dz \equiv \prod_{i=1}^N dz^i$ to the modulus $|dz|$ and the phase $e^{i\varphi(z)}$,

$$dz = |dz| e^{i\varphi(z)}, \quad (2.3)$$

and rewrite $dz e^{-S(z)}$ as⁵

$$dz e^{-S(z)} = |dz| e^{-\text{Re } S(z)} e^{i\theta(z)} \quad (e^{i\theta(z)} \equiv e^{i\varphi(z)} e^{-i \text{Im } S(z)}), \quad (2.4)$$

from which (2.2) will be written as a ratio of reweighted integrals on Σ :

$$\langle \mathcal{O}(x) \rangle = \frac{\int_{\Sigma} dz e^{-S(z)} \mathcal{O}(z)}{\int_{\Sigma} dz e^{-S(z)}} = \frac{\langle e^{i\theta(z)} \mathcal{O}(z) \rangle_{\Sigma}}{\langle e^{i\theta(z)} \rangle_{\Sigma}} \quad (2.5)$$

⁴We also assume that there is no multimodal problem on the original configuration space $\mathbb{R}^N (\subset \mathbb{C}^N)$ with respect to $\text{Re } S(x)$.

⁵Note that $|dz|$ agrees with the volume element associated with the induced metric on Σ in $\mathbb{R}^{2N} (= \mathbb{C}^N)$.

with

$$\langle f(z) \rangle_{\Sigma} \equiv \frac{1}{Z_{\Sigma}} \int_{\Sigma} |dz| e^{-\text{Re} S(z)} f(z) \quad (Z_{\Sigma} = \int_{\Sigma} |dz| e^{-\text{Re} S(z)}). \quad (2.6)$$

We then generate a sample $\{z^{(k)}\}_{k=1, \dots, N_{\text{conf}}}$ from the distribution $e^{-\text{Re} S(z)}/Z_{\Sigma}$,⁶ and estimate $\langle f(z) \rangle_{\Sigma}$ as a sample average,

$$\langle f(z) \rangle_{\Sigma} \approx \frac{1}{N_{\text{conf}}} \sum_{k=1}^{N_{\text{conf}}} f(z^{(k)}) \equiv \overline{f(z)}, \quad (2.7)$$

from which $\langle \mathcal{O}(x) \rangle$ is estimated as⁷

$$\langle \mathcal{O}(x) \rangle = \frac{\langle e^{i\theta(z)} \mathcal{O}(z) \rangle_{\Sigma}}{\langle e^{i\theta(z)} \rangle_{\Sigma}} \approx \frac{\overline{e^{i\theta(z)} \mathcal{O}(z)}}{\overline{e^{i\theta(z)}}} \equiv \bar{\mathcal{O}}. \quad (2.8)$$

In a class of Lefschetz thimble methods (see, e.g., [9, 10, 11, 12]), continuous deformations of integration region are made according to the antiholomorphic flow equation:

$$\dot{z}_t^i = [\partial_i S(z_t)]^*, \quad z_{t=0}^i = x^i, \quad (2.9)$$

which defines a map from $x \in \mathbb{R}^N$ to $z = z_t(x) \in \mathbb{C}^N$. Since $(d/dt) S(z_t) = |\partial_i S(z_t)|^2 \geq 0$, the real part $\text{Re} S(z_t)$ always increase along the flow except at critical points z_{σ} (where $\partial_i S(z_{\sigma}) = 0$), while the imaginary part $\text{Im} S(z_t)$ is kept constant. In the limit $t \rightarrow \infty$, $\Sigma_t \equiv z_t(\mathbb{R}^N)$ will approach a union of Lefschetz thimbles, on each of which $\text{Im} S(z)$ is constant, and thus the sign problem is expected to disappear there (except for a possible residual and/or global sign problem).⁸ However, for large t there arises a new problem, multimodal (ergodicity) problem, because the potential barriers between different thimbles become infinitely high as t increases.

In the tempered Lefschetz thimble method (TLTM) [11, 12], we resolve the dilemma between the sign problem (severe at small flow times) and the ergodicity problem (severe at large flow times) by tempering the system with the flow time.⁹ The algorithm consists

⁶When we consider probability densities $p(z)$ at $z \in \Sigma$, they are always with respect to the measure $|dz|$. The measure $|dz|$ will also be written as $(dz)_{\parallel}$ in later discussions. A transition from $p(z)$ to $\tilde{p}(z)$ with transition probability $P(z'|z)$ is then expressed as

$$\tilde{p}(z') = \int_{\Sigma} |dz| P(z'|z) p(z) \quad (z' \in \Sigma).$$

⁷The statistical errors of $\overline{f(z)}$ and the ratio $\bar{\mathcal{O}}$ will be estimated using the binning-Jackknife method (with autocorrelations taken into account).

⁸In the case when the action diverges at some points in \mathbb{C}^N (such as zeros of the fermion determinant), Σ_t should be understood to represent $z_t(\mathbb{R}^N)$ with these points removed.

⁹As a tempering algorithm, we adopt the parallel tempering (also called the replica exchange MCMC method) [24, 25, 26] because then we need not specify the probability weight factors at various flow times and because most of relevant steps can be done in parallel processes.

of three steps. (1) First, we introduce a set of configuration spaces, $\{\Sigma_{t_a}\}$ ($a = 0, 1, \dots, A$), with $t_0 = 0 < t_1 < \dots < t_A = T$. We often call Σ_{t_a} the a -th replica. Here, a possible criterion for choosing the maximum flow time T is that the sign average $|\langle e^{i\theta(z)} \rangle_{\Sigma_T}|$ is $O(1)$ without tempering. (2) We then construct a Markov chain that drives the enlarged system $\Sigma_{\text{tot}} \equiv \Sigma_{t_0} \times \Sigma_{t_1} \times \dots \times \Sigma_{t_A} = \{\vec{z} = (z_a)\}$ to global equilibrium with the distribution $p_{\text{eq}}(\vec{z}) \propto \prod_a \exp[-\text{Re } S(z_a)]$. (3) After the system is well relaxed to global equilibrium, we estimate the expectation value on Σ_{t_a} [see (2.8)] by using the subsample at replica a , $\{z_a^{(k)}\}_{k=1,2,\dots,N_{\text{conf}}}$, that is retrieved from the total sample $\{\vec{z}^{(k)} = (z_0^{(k)}, z_1^{(k)}, \dots, z_A^{(k)})\}_{k=1,2,\dots,N_{\text{conf}}}$:

$$\frac{\langle e^{i\theta(z_a)} \mathcal{O}(z_a) \rangle_{\Sigma_{t_a}}}{\langle e^{i\theta(z_a)} \rangle_{\Sigma_{t_a}}} \approx \frac{\overline{e^{i\theta(z_a)} \mathcal{O}(z_a)}}{\overline{e^{i\theta(z_a)}}} \equiv \bar{\mathcal{O}}_a. \quad (2.10)$$

Since the left-hand side of (2.10) is independent of a due to Cauchy's theorem, the ratio $\bar{\mathcal{O}}_a$ at large a 's (where the sign problem is relaxed) should yield the same value within the statistical error margin if the system is well in global equilibrium. Conversely, the requirement of a -independence ensures the sample to be in global equilibrium with a sufficient sample size (together with the correctness of the employed numerical method), and is the basis of the following algorithm for precise estimation [12]. First, we continue the sampling until we find some range of a , in which (i) $|\overline{e^{i\theta(z_a)}}|$ are well above $1/\sqrt{2N_{\text{conf}}}$ (the values for the uniform distribution of phases) and (ii) $\bar{\mathcal{O}}_a$ take the same value within the statistical error margin. Then, we estimate $\langle \mathcal{O} \rangle$ by using the χ^2 fit (using covariance) of $\{\bar{\mathcal{O}}_a\}$ in this region with a constant function of a . Global equilibrium and the sufficiency of the sample size are checked by looking at the optimized value of χ^2/DOF .

2.2. Real representation for complex variables

In the following sections, we mainly use the real representation for complex variables, where a point $z = (z^i) = x + iy \in \mathbb{C}^N$ ($i = 1, \dots, N$) is expressed by $z = (z^I) \equiv (x, y)^T \in \mathbb{R}^{2N}$ ($I = 1, \dots, 2N$).¹⁰ Accordingly, a complex column vector $v = (v^i) = v_R + iv_I \in \mathbb{C}^N$ will be written as a real vector $v = (v^I) \equiv (v_R, v_I)^T \in \mathbb{R}^{2N}$. Under this identification, an $N \times N$ complex matrix $A = (A_{ij}) = A_R + iA_I$ will be given as a $2N \times 2N$ matrix,

$$A = (A_{IJ}) \equiv \begin{pmatrix} A_R & -A_I \\ A_I & A_R \end{pmatrix}. \quad (2.11)$$

We write the multiplication of i (imaginary unit) and the complex conjugation, respectively, as

$$\hat{i} \equiv \begin{pmatrix} 0 & -1_N \\ 1_N & 0 \end{pmatrix}, \quad \hat{C} \equiv \begin{pmatrix} 1_N & 0 \\ 0 & -1_N \end{pmatrix}, \quad (2.12)$$

¹⁰We use the same symbol for both representations to avoid introducing many redundant symbols. Which representation is used should be obvious from the context, and otherwise it will be clearly stated.

and introduce the projectors to the real and imaginary parts, respectively, as

$$\widehat{\text{Re}} \equiv \frac{1}{2} (1 + \hat{C}) = \begin{pmatrix} 1_N & 0 \\ 0 & 0 \end{pmatrix}, \quad \widehat{\text{Im}} \equiv \frac{1}{2} (1 - \hat{C}) = \begin{pmatrix} 0 & 0 \\ 0 & 1_N \end{pmatrix}. \quad (2.13)$$

2.3. Outline for the implementation of HMC on TLTM

We will often abbreviate flowed surfaces $\Sigma_{t_a} = \{z_a\}$ as Σ_a ($a = 0, 1, \dots, A$) to simplify expressions. In the parallel tempering, the total configuration space is given by

$$\Sigma_{\text{tot}} \equiv \Sigma_0 \times \dots \times \Sigma_A = \{\vec{z} = (z_a)\}, \quad (2.14)$$

which we regard as a complex of playgrounds with $A + 1$ zones for the same number of molecules, where each molecule moves around from a zone to another zone under the condition that any two molecules cannot be in the same zone.¹¹ In order to implement an HMC algorithm on the tempered system, we introduce to each replica Σ_a the phase space $T^*\Sigma_a = \{\zeta_a = (z_a, \pi_a)\}$ and the Hamiltonian

$$H_a(\zeta_a) \equiv \frac{\pi_a^2}{2M_a} + V(z_a), \quad (2.15)$$

where $\pi_a^2/2M_a \equiv (1/2) (M_a^{-1})^{IJ} \pi_{a,I} \pi_{a,J}$ and $V(z_a) \equiv \text{Re } S(z_a)$. M_a is constant and will be set to be $(M_a)_{IJ} = \sigma_a^2 \delta_{IJ}$.

We construct a molecular dynamics on each phase space $T^*\Sigma_a$ (to be explained in detail in the next section), that defines a one-body motion from $\zeta_a \in T^*\Sigma_a$ to $\Phi_a(\zeta_a) \in T^*\Sigma_a$. Φ_a will be designed such that it is volume-preserving and reversible, and thus the transition probability¹²

$$\mathbb{P}_a^{(1)}(\zeta'_a | \zeta_a) \equiv \min(1, e^{-H_a(\zeta'_a) + H_a(\zeta_a)}) \delta(\zeta'_a - \Phi_a(\zeta_a)) \quad (\zeta'_a \neq \zeta_a) \quad (2.16)$$

satisfies the relation

$$\mathbb{P}_a^{(1)}(\zeta'_a | \zeta_a) e^{-H_a(\zeta_a)} = \mathbb{P}_a^{(1)}(\zeta_a^T | \zeta'_a{}^T) e^{-H_a(\zeta'_a)} \quad (\zeta'_a \neq \zeta_a), \quad (2.17)$$

where $\zeta^T \equiv (z, -\pi)$ for $\zeta = (z, \pi)$ and we have used the fact $H_a(\zeta_a^T) = H_a(\zeta_a)$.

We then define the transition probability on each replica:¹³

$$P_a^{(1)}(z'_a | z_a) \equiv c_a \int d\pi'_a d\pi_a \mathbb{P}_a^{(1)}(z'_a, \pi'_a | z_a, \pi_a) e^{-\pi_a^2/2M_a} \quad (2.18)$$

¹¹ Note that the index a labels the zones, not the molecules.

¹² The diagonal elements are determined automatically by the probability conservation $\int d\zeta'_a \mathbb{P}_a^{(1)}(\zeta'_a | \zeta_a) =$

1. This comment will be applied to similar expressions in what follows.

¹³ $d\pi_a$ is the volume element of $T_{z_a}^*\Sigma_a$ and will be denoted by $(d\pi_a)_\parallel$ when π_a is an element in $T_{z_a}^*\mathbb{R}^{2N}$.

with $c_a \equiv [\int d\pi_a e^{-\pi_a^2/2M_a}]^{-1}$. $P_a^{(1)}$ satisfies the following detailed balance condition:

$$P_a^{(1)}(z'_a|z_a) e^{-V(z_a)} = P_a^{(1)}(z_a|z'_a) e^{-V(z'_a)}. \quad (2.19)$$

We also introduce a two-body evolution that maps $(z_a, z_b) \in \Sigma_a \times \Sigma_b$ to $(z'_a, z'_b) \in \Sigma_a \times \Sigma_b$ with the probability $P_{ab}^{(2)}(z'_a, z'_b|z_a, z_b)$ satisfying the relation

$$P_{ab}^{(2)}(z'_a, z'_b|z_a, z_b) e^{-V(z_a)-V(z_b)} = P_{ab}^{(2)}(z_a, z_b|z'_a, z'_b) e^{-V(z'_a)-V(z'_b)}. \quad (2.20)$$

By combining $P_a^{(1)}$ and $P_{ab}^{(2)}$, one can construct a Markov chain such that its transition probability $P_{\text{tot}}(\vec{z}'|\vec{z})$ gives the desired equilibrium distribution $p_{\text{eq}}(\vec{z}) \propto \prod_a e^{-V(z_a)}$.

In the following sections, we define a molecular dynamics on each replica (section 3) and then give an explicit algorithm for HMC on TLTM (section 4).

3. Molecular dynamics on flowed surfaces

In this section, we first give a brief review of molecular dynamics on a general constrained surface Σ , and then discuss molecular dynamics on a flowed surface $\Sigma = \Sigma_t$ that is obtained as a time slice from the antiholomorphic gradient flow with flow time t .

3.1. Molecular dynamics on a general constrained surface

Let Σ be an m -dimensional surface in \mathbb{R}^{2N} ($= \mathbb{C}^N$), which we assume is given by a set of constraint equations¹⁴

$$\phi^r(z) = 0 \quad (r = 1, \dots, 2N - m). \quad (3.1)$$

At point $z \in \Sigma$, we choose a basis of the tangent space $T_z \Sigma$ and denote it by $E_\alpha = (E_\alpha^I)$ ($\alpha = 1, \dots, m$), from which we define the metric $g_{\alpha\beta} \equiv \delta_{IJ} E_\alpha^I E_\beta^J$. We also introduce a basis $F_r = (F_r^I)$ of the normal space $N_z \Sigma$.

Let $T^*\mathbb{R}^{2N} = \{\zeta = (z, \pi)\}$ be the phase space on \mathbb{R}^{2N} with a separable Hamiltonian of the form

$$H(\zeta) = H(z, \pi) = \frac{1}{2} (M^{-1})^{IJ} \pi_I \pi_J + V(z), \quad (3.2)$$

where the positive symmetric mass matrix $M = (M_{IJ})$ is assumed to be constant.¹⁵ A motion on Σ defines a motion in the reduced phase space

$$T^*\Sigma \equiv \{\zeta = (z, \pi) \in T^*\mathbb{R}^{2N} \mid \phi^r(z) = 0, (M^{-1}\pi)^I \partial_{z^I} \phi^r(z) = 0\}. \quad (3.3)$$

¹⁴Later we will set $m = N$.

¹⁵We assume that M satisfies the condition $M_{IJ} E_\alpha^I F_r^J = 0$, which ensures that $(M^{-1})^{IJ} \pi_J$ is on the tangent space $T_z \Sigma$ for $\pi = (\pi_I) \in T_z^* \Sigma$.

The symplectic structure of $T^*\Sigma$ is defined by the induced symplectic form

$$\omega \equiv d\pi_I \wedge dz^I|_{T^*\Sigma}, \quad (3.4)$$

from which we define the volume element dV on $T^*\Sigma$ by

$$dV \equiv \frac{\omega^m}{m!}. \quad (3.5)$$

When $d^{2N}z \equiv \prod_I dz^I$ and $d^{2N}\pi \equiv \prod_I d\pi_I$ are orthogonally decomposed as (see Fig. 1)

$$d^{2N}z = (dz)_\parallel (dz)_\perp, \quad d^{2N}\pi = (d\pi)_\parallel (d\pi)_\perp, \quad (3.6)$$

one can easily show that

$$dV = (dz)_\parallel (d\pi)_\parallel. \quad (3.7)$$

Note that $(dz)_\parallel = |dz|$ and $(d\pi)_\parallel$ corresponds to $d\pi$ in subsection 2.3. If we introduce local

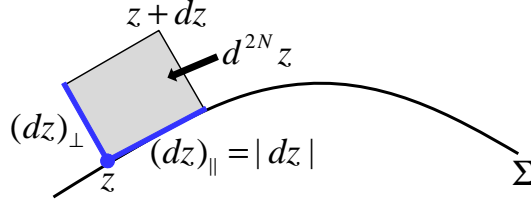


Figure 1: Orthogonal decomposition of $d^{2N}z$.

coordinates $\xi = (\xi^\alpha)$ on Σ , then we can choose the basis of $T_z\Sigma$ to be $E_\alpha^I = \partial z^I / \partial \xi^\alpha$. It is convenient to define the projected components η_α for arbitrary momentum $\tilde{\pi} = (\tilde{\pi}_I) \in T_z^*\mathbb{R}^{2N}$:

$$\eta_\alpha \equiv \tilde{\pi}_I E_\alpha^I. \quad (3.8)$$

One can easily show that

$$\omega = d\eta_\alpha \wedge d\xi^\alpha, \quad (3.9)$$

and thus the volume element can be expressed as¹⁶

$$dV = \prod_\alpha d\xi^\alpha d\eta_\alpha. \quad (3.10)$$

One can also show that the projection of $\tilde{\pi}$ to $\pi = \tilde{\pi}_\parallel$ is given by

$$\pi_I = \eta_\alpha E_I^\alpha = \tilde{\pi}_J \mathcal{P}_I^J, \quad (3.11)$$

¹⁶With the local coordinates, each factor in (3.7) is written as $(dz)_\parallel = |dz| = \sqrt{g} \prod_\alpha d\xi^\alpha$ and $(d\pi)_\parallel = (1/\sqrt{g}) \prod_\alpha d\eta_\alpha$ with $g = \det(g_{\alpha\beta}(\xi))$.

where $E_I^\alpha \equiv g^{\alpha\beta} \delta_{IJ} E_\beta^J$ [$(g^{\alpha\beta}) \equiv (g_{\alpha\beta})^{-1}$] and $\mathcal{P}_I^J \equiv E_\alpha^J E_I^\alpha$.

In the continuous language, a motion $\zeta(s) = (z(s), \pi(s))$ in $T^*\Sigma$ is described by the following equations with Lagrange multipliers λ_r :

$$\partial_s z^I = \partial_{\pi_I} H = (M^{-1}\pi)^I, \quad (3.12)$$

$$\partial_s \pi_I = -\partial_{z^I} H - \lambda_r \partial_{z^I} \phi^r(z) = -\partial_{z^I} V(z) - \lambda_r \partial_{z^I} \phi^r(z), \quad (3.13)$$

$$0 = \phi^r(z), \quad (3.14)$$

$$0 = (M^{-1}\pi)^I \partial_{z^I} \phi^r(z). \quad (3.15)$$

Note that (3.15) (obtained by taking the derivative of (3.14) with respect to s) means that the velocity $\partial_s z = M^{-1}\pi$ is tangent to Σ . Equations (3.12)–(3.15) have the following properties: (1) symplecticity: The induced symplectic form (3.4) does not change under the motion, $\partial_s \omega = 0$, and thus the volume element dV is preserved. (2) reversibility: For any motion $(z, \pi) \xrightarrow{s} (z', \pi')$ obtained by integrating (3.12)–(3.15), its time-reversed motion $(z', -\pi') \xrightarrow{s} (z, -\pi)$ is also a solution. (3) energy conservation: $H(z', \pi') = H(z, \pi)$.

RATTLE [17, 18] is a discrete version of the above molecular dynamics, and generates a one-step motion from $(z, \pi) \in T^*\Sigma$ to $(z', \pi') \equiv \Phi_{\Delta s}(z, \pi) \in T^*\Sigma$ as follows:

$$\pi_{1/2} = \pi - \frac{\Delta s}{2} \partial V(z) - \frac{\Delta s}{2} \lambda_r^{(1)} \partial \phi^r(z), \quad (3.16)$$

$$z' = z + \Delta s (M^{-1} \pi_{1/2}), \quad (3.17)$$

$$0 = \phi^r(z'), \quad (3.18)$$

$$\pi' = \pi_{1/2} - \frac{\Delta s}{2} \partial V(z') - \frac{\Delta s}{2} \lambda_r^{(2)} \partial \phi^r(z'), \quad (3.19)$$

$$0 = (M^{-1}\pi') \cdot \partial \phi^r(z'), \quad (3.20)$$

where Δs is the step size and $\partial V(z) \equiv (\partial_{z^I} V(z))$. Note that there appear two Lagrange multipliers. $\lambda_r^{(1)}$ is determined so that the new configuration z' is on Σ [$z' \in \Sigma$, eq. (3.18)], while $\lambda_r^{(2)}$ is determined so that π' is in the tangential direction [$\pi' \in T_{z'}^*\Sigma$, eq. (3.20)]. One can easily check that $\Phi_{\Delta s}$ is symplectic ($d\pi' \wedge dz'|_{T^*\Sigma} = d\pi \wedge dz|_{T^*\Sigma}$) and reversible [if $(z', \pi') = \Phi_{\Delta s}(z, \pi)$ then $(z, -\pi) = \Phi_{\Delta s}(z', -\pi')$ with the interchange of $\lambda^{(1)}$ and $\lambda^{(2)}$], and preserves the energy to second order:

$$H(z', \pi') = H(z, \pi) + O(\Delta s^3). \quad (3.21)$$

We need to rewrite the above RATTLE process when, as in Lefschetz thimble methods [7], we do not know explicit functional forms of the constraint functions $\phi^r(z)$ except for the bases of the tangent and the normal spaces at z [$E_\alpha = (E_\alpha^I)$ and $F_r = (F_r^I)$, respectively]. This rewriting can be done in the following way by using the orthogonal projector $\mathcal{P}(z) = (\mathcal{P}_J^I(z))$ from $T_z^*\mathbb{R}^{2N}$ to $T_z^*\Sigma$ (see Fig. 2):¹⁷

¹⁷We owe much of the discussions for RATTLE on a flowed surface to [19], where a generalization is made from the RATTLE on a single Lefschetz thimble [7].

crucial point here is that, although we do not know explicit functional forms of $\phi^\alpha(z)$, there is a one-to-one correspondence between the points $z = (z^I) \in \Sigma_t$ and those $x = (x^\alpha) \in \mathbb{R}^N$ with the relation $z = z_t(x)$. Furthermore, the bases of the tangent and normal spaces at $z = z_t(x)$ can be given explicitly as

$$E_\alpha^I(x) \equiv \partial z_t^I(x)/\partial x^\alpha, \quad F_\alpha^I(x) \equiv (\hat{i} E_\alpha(x))^I \quad (I = 1, \dots, 2N), \quad (3.27)$$

whose complex representations are $E_\alpha^i = \partial z_t^i(x)/\partial x^\alpha$ and $F_\alpha^i = i E_\alpha^i$ ($i = 1, \dots, N$) [7]. Note that $(E_\alpha^i(x))$ is nothing but the (complex-valued) Jacobian matrix $J(x) = J_t(x) = (\partial z_t^i(x)/\partial x^\alpha)$, that obeys the following differential equation in the complex representation [9] (see also footnote 2 of [11]):

$$\dot{J}_t = [H(z_t) \cdot J_t]^*, \quad J_{t=0} = 1_N \quad (3.28)$$

with $H(z) \equiv (\partial_i \partial_j S(z))$. The real representation of $J(x) = J_R(x) + iJ_I(x)$ is in turn given by²⁰

$$J(x) = (J_A^I(x)) \equiv \begin{pmatrix} (J_R(x))^i_\alpha & -(J_I(x))^i_\alpha \\ (J_I(x))^i_\alpha & (J_R(x))^i_\alpha \end{pmatrix} = (E_\alpha(x), F_\alpha(x)) \quad (A = 1, \dots, 2N). \quad (3.29)$$

The condition that $z' \in \Sigma_t \subset \mathbb{R}^{2N}$ for a given $z = z_t(x)$ [eq. (3.23)] is equivalent to that there be a vector $u = (u^\alpha) \in \mathbb{R}^N$ such that z' can be written as $z' = z_t(x + u)$. Together with the need to find $\lambda = (\lambda^\alpha) \in \mathbb{R}^N$, our requirement can be expressed as the following $2N$ equations for $2N$ unknown variables u^α, λ^α ($\alpha = 1, \dots, N$):

$$\begin{aligned} 0 &= z_t^I(x + u) - \tilde{z}^I + F_\alpha^I(z) \lambda^\alpha \\ &= z_t^I(x + u) - z_t^I(x) - \Delta s (M^{-1} \pi)^I + \frac{\Delta s^2}{2} (M^{-1} \partial V(z))^I + F_\alpha^I(z) \lambda^\alpha \\ &\equiv f^I(u, \lambda; x). \end{aligned} \quad (3.30)$$

This equation can be solved iteratively for

$$w = (w^A) = \begin{pmatrix} u^\alpha \\ \lambda^\alpha \end{pmatrix} \quad (3.31)$$

with Newton's method. Namely, starting from an initial guess $w_0 = (w_0^A)$, we obtain a sequence $w_k \rightarrow w_{k+1} = w_k + \Delta w$ by solving the linear equation

$$\left. \frac{\partial f^I}{\partial w^A} \right|_{w_k} \Delta w^A = -f^I(w_k). \quad (3.32)$$

²⁰With (3.28) and (3.29) the orthogonality between $E_\alpha = (E_\alpha^I)$ and $F_\alpha = (F_\alpha^I)$ can be shown as follows [7]. We first note that their inner products $E_\alpha \cdot F_\beta \equiv \delta_{IJ} E_\alpha^I F_\beta^J$ can be written as $-\text{Im} (J_t^\dagger J_t)_{\alpha\beta}$, and that they do not depend on t due to the first equation of (3.28). We then conclude that $E_\alpha \cdot F_\beta$ must vanish due to the initial condition $J_{t=0} = 1_N$, for which $-\text{Im} (J_t^\dagger J_t)|_{t=0} = 0$.

Here, from the explicit form of f^I , we find that

$$\frac{\partial f^I}{\partial u^\alpha} = \frac{\partial z^I(x+u)}{\partial u^\alpha} = \frac{\partial z^I(x)}{\partial x^\alpha} \Big|_{x+u} = E_\alpha^I(x+u), \quad (3.33)$$

$$\frac{\partial f^I}{\partial \lambda^\alpha} = F_\alpha^I(x), \quad (3.34)$$

and thus the recursive equation can be written as

$$(E_\alpha(x+u_k), F_\alpha(x)) \begin{pmatrix} \Delta u^\alpha \\ \Delta \lambda^\alpha \end{pmatrix} = -f(w_k), \quad (3.35)$$

or equivalently,

$$\begin{pmatrix} J_R(x+u_k) & -J_I(x) \\ J_I(x+u_k) & J_R(x) \end{pmatrix} \begin{pmatrix} \Delta u \\ \Delta \lambda \end{pmatrix} = -f(w_k). \quad (3.36)$$

The linear equation (3.36) can be solved in two ways. One is to directly obtain all the matrix elements of the Jacobian matrices $J(x) = J_R(x) + i J_I(x)$ and $J(x+u_k) = J_R(x+u_k) + i J_I(x+u_k)$ by numerically integrating (2.9) and (3.28) and then to obtain the solution $\Delta w = (\Delta u, \Delta \lambda)^T$ with a direct method such as the LU decomposition. The other method is to use an iterative method such as GMRES [27] or BiCGStab [28] without calculating the matrix elements explicitly (as in [29]). The reason why such a method is possible here is that the left-hand side of (3.36) can be rewritten as

$$\begin{pmatrix} J_R(x+u_k) & -J_I(x+u_k) \\ J_I(x+u_k) & J_R(x+u_k) \end{pmatrix} \begin{pmatrix} \Delta u \\ 0 \end{pmatrix} + i \begin{pmatrix} J_R(x) & -J_I(x) \\ J_I(x) & J_R(x) \end{pmatrix} \begin{pmatrix} \Delta \lambda \\ 0 \end{pmatrix}, \quad (3.37)$$

and each term can be evaluated by numerically integrating the following differential equations for $z_t = (z_t^I)$ and a vector $v_t = (v_t^I)$ (not for a matrix):

$$\dot{z}_t = \hat{C} \partial \text{Re} S(z_t), \quad (3.38)$$

$$\dot{v}_t = \hat{C} H(z_t) v_t = \begin{pmatrix} H_R(z_t) & -H_I(z_t) \\ -H_I(z_t) & -H_R(z_t) \end{pmatrix} v_t \quad (3.39)$$

with the initial conditions $z_0 = x + u_k$ and $v_0 = (\Delta u, 0)^T$ or $z_0 = x$ and $v_0 = (\Delta \lambda, 0)^T$. Note that the complex representations of (3.38) and (3.39) for $z_t = (z_t^i)$, $v_t = (v_t^i) \in \mathbb{C}^N$ are given, respectively, by

$$\dot{z}_t^i = [\partial_i S(z_t)]^*, \quad \dot{v}_t^i = [H_{ij}(z_t) v_t^j]^*. \quad (3.40)$$

The initial conditions are then given by $z_0^i = x^i + u_k^i$ and $v_0^i = \Delta u^i$ or $z_0^i = x^i$ and $v_0^i = \Delta \lambda^i$ for $\Delta u, \Delta \lambda \in \mathbb{R}^N$.

In the procedure given in subsection 3.1, one needs to use the projector $\mathcal{P}(z) = (\mathcal{P}^I_J(z))$ that projects $\tilde{\pi} \in T_z^* \mathbb{R}^{2N}$ to $\pi = \tilde{\pi} \mathcal{P}(z) \in T_z^* \Sigma_t$ at $z = z_t(x)$, or equivalently, that projects $\tilde{v} \equiv M^{-1} \tilde{\pi} \in T_z \mathbb{R}^{2N}$ to $v \equiv M^{-1} \pi = \mathcal{P}(z) \tilde{v} \in T_z \Sigma_t$ at $z = z_t(x)$. The projection can also be given in two ways. When the matrix elements of $J(x)$ are known explicitly as in the direct method given in the previous paragraph, the matrix $\mathcal{P} = (\mathcal{P}^I_J = E^I_\alpha E^\alpha_J)$ can also be calculated explicitly as

$$\mathcal{P} = (E^I_\alpha) (E^\alpha_J) = (E^I_\alpha, F^I_\alpha) \begin{pmatrix} \delta^\alpha_\beta & 0 \\ 0 & 0 \end{pmatrix} \begin{pmatrix} E^\beta_J \\ F^\beta_J \end{pmatrix} = J(x) \widehat{\text{Re}} J^{-1}(x), \quad (3.41)$$

whose complex representation is given by a map $\mathbb{C}^N \ni \tilde{v} \mapsto v = J(x) \text{Re} [J^{-1}(x) \tilde{v}] \in \mathbb{C}^N$.²¹ The other method does not require an explicit knowledge of the matrix elements of $J(x)$ (as in [29]). We here demonstrate this procedure in the complex representation. We first look for two real column vectors $a, b \in \mathbb{R}^N$ such that they satisfy a linear equation

$$J(x) a + i J(x) b = \tilde{v} \in \mathbb{C}^N. \quad (3.42)$$

Here, $J(x) a$ and $J(x) b$ are obtained by numerically integrating (3.40) with the initial conditions $(z_0, v_0) = (x, a)$ and $(z_0, v_0) = (x, b)$, respectively. The linear equation (3.42) can be solved for a, b with an iterative method. Once a and b are obtained, v is given by $J(x) a$ (which we already have in the above process) because the formal solution for a is given by $a = \text{Re} [J^{-1}(x) \tilde{v}]$.

We summarize the algorithm for a molecular dynamics on $T^* \Sigma_t$ that updates a configuration from $\zeta = (z, \pi) \in T^* \Sigma_t$ with $z = z_t(x)$ to $\zeta' = (z', \pi') = \Phi_{\Delta s}(z, \pi) \in T^* \Sigma_t$ with $z' = z_t(x')$. Every step below will be mostly given in the real representation, which can be readily translated to the complex representation.²²

Step 1. For $\zeta = (z, \pi) \in T^* \Sigma_t$ with $z = z_t(x)$, we find $w = (u, \lambda)^T = ((u^\alpha), (\lambda^\alpha))^T$ ($\alpha = 1, \dots, N$) that satisfies (3.30). The equation can be solved iteratively, $w_k \rightarrow w_{k+1} = w_k + \Delta w$, with Newton's method, starting from an initial guess $w_0 = (u_0, \lambda_0)^T$

²¹This expression first appeared in [7] as the projection to the tangent spaces to a Lefschetz thimble.

²²When $M_{IJ} = \sigma^2 \delta_{IJ}$, eqs. (3.22)–(3.26) have the following complex representations for $z = (z^i = x^i + i y^i)$ and $\pi = (\pi_i = \pi_{i,x} + i \pi_{i,y})$ with $\partial S(z) \equiv (\partial_i S(z))$ and $J = (\partial z^i / \partial x^\alpha)$:

$$\begin{aligned} \tilde{z} &= z + (\Delta s / \sigma^2) \pi - (\Delta s^2 / 2 \sigma^2) [\partial S(z)]^*, \\ z' &= \tilde{z} - i J(z) \lambda \quad (\lambda \in \mathbb{R}^N), \\ \pi_{1/2} &= (\sigma^2 / \Delta s) (z' - z), \\ \tilde{\pi}' &= \pi_{1/2} - (\Delta s / 2) [\partial S(z')]^*, \\ \pi' &= J(z') \text{Re} (J^{-1}(z') \tilde{\pi}'). \end{aligned}$$

and solving the linear equation (3.36) to obtain $\Delta w = (\Delta u, \Delta \lambda)^T$. Equation (3.36) can be solved with either of a direct method or an iterative method. After $w = (u, \lambda)^T$ is obtained, we set $x' \equiv x + u$ and $z' \equiv z_t(x')$.

Step 2. Define

$$\pi_{1/2} \equiv \frac{1}{\Delta s} M(z' - z), \quad (3.43)$$

and set

$$\tilde{\pi}' \equiv \pi_{1/2} - \frac{\Delta s}{2} \partial V(z'). \quad (3.44)$$

Step 3. Project $\tilde{v}' \equiv M^{-1}\tilde{\pi}'$ to $v' = \mathcal{P}(z')\tilde{v}' \in T_{z'}\Sigma_t$ to obtain $\pi' = Mv' \in T_{z'}^*\Sigma_t$. The projection can be made with a direct method when the matrix elements of $J(x')$ are known explicitly, or with an iterative method.

In practice, since Δs is finite, it can happen, for z close to zeros of the weight $e^{-S(z)}$, that one cannot find a solution $z' = z_t(x')$ to (3.32) anywhere in \mathbb{C}^N or can only find a solution in a region beyond the zeros (see appendix A for detailed discussions). When this happens, we replace $\Phi_{\Delta s}$ by a *momentum flip* Ψ that is defined by²³

$$\Psi(z, \pi) = (z, -\pi). \quad (3.45)$$

Note that Ψ is also volume-preserving [i.e., $(dz')_{\parallel}(d\pi')_{\parallel} = (dz)_{\parallel}(d\pi)_{\parallel}$ for $(z', \pi') = \Psi(z, \pi)$] and reversible [i.e., if $\Psi(z, \pi) = (z', \pi')$ then $\Psi(z', -\pi') = (z, -\pi)$]. To understand the reversibility, consider a move of a molecule in the forward and backward directions in s , each consisting of three steps (see Fig. 3):

$$\text{forward: } (z_0, \pi_0) \xrightarrow{\Phi_{\Delta s}} (z_1, \pi_1) \xrightarrow{\Psi} (z_2, \pi_2) \xrightarrow{\Phi_{\Delta s}} (z_3, \pi_3), \quad (3.46)$$

$$\text{backward: } (\tilde{z}_0, \tilde{\pi}_0) \xrightarrow{\Phi_{\Delta s}} (\tilde{z}_1, \tilde{\pi}_1) \xrightarrow{\Psi} (\tilde{z}_2, \tilde{\pi}_2) \xrightarrow{\Phi_{\Delta s}} (\tilde{z}_3, \tilde{\pi}_3) \quad (3.47)$$

with $(\tilde{z}_0, \tilde{\pi}_0) \equiv (z_3, -\pi_3)$. There, we assume that a move from z_1 with π_1 is prohibited by a prescribed condition. We thus flip the momentum from π_1 to $\pi_2 = -\pi_1$, and the molecule arrives at z_3 with π_3 . As for the backward move starting from $\tilde{z}_0 = z_3$ with $\tilde{\pi}_0 = -\pi_3$, it will arrive at $\tilde{z}_1 = z_2 (= z_1)$ with $\tilde{\pi}_1 = -\pi_2 (= \pi_1)$ thanks to the reversibility of $\Phi_{\Delta s}$. Then the further move with $\tilde{\pi}_1$ must be prohibited by the same condition that prohibited the further move from z_1 with π_1 . Then we make a momentum flip from $\tilde{\pi}_1$ to $\tilde{\pi}_2 = -\tilde{\pi}_1$, and the molecule will arrive at \tilde{z}_3 which must coincide with z_0 again thanks to the reversibility

²³Note that such an aggressive withdrawal is allowed as an algorithm because a detour to go around zeros are provided by the tempering.

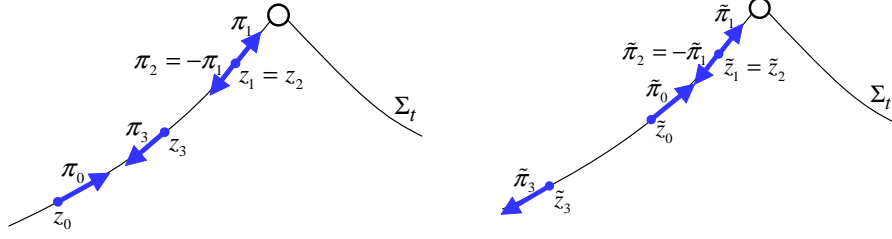


Figure 3: Moves on Σ_t near a zero of $e^{-S(z)}$ (indicated by a circle). (Left) An original forward move with a momentum flip at z_1 . (Right) The time-reversed backward move.

of Φ_{Δ_s} . We thus see that the reversibility holds for the whole process with the relation $(\tilde{z}_n, \tilde{\pi}_n) = (z_{3-n}, -\pi_{3-n})$.

Due to the volume-preservation and the reversibility of Φ_{Δ_s} and Ψ , the transition probability

$$\mathbb{P}^{(1)}(\zeta'|\zeta) \equiv \min(1, e^{-H(\zeta') + H(\zeta)}) \delta(\zeta' - \Phi_{\Delta_s}^n(\zeta)) \quad (\zeta' \neq \zeta) \quad (3.48)$$

satisfies the following relation [see (2.16) and (2.17)]:

$$\mathbb{P}^{(1)}(\zeta'|\zeta) e^{-H(\zeta)} = \mathbb{P}^{(1)}(\zeta^T|\zeta'^T) e^{-H(\zeta')} \quad (\zeta' \neq \zeta) \quad (3.49)$$

even when the partial replacements from Φ_{Δ_s} to Ψ are made. In the following, we only use the symbol Φ_{Δ_s} with the understanding that it will be replaced by Ψ when necessary.

4. HMC on TLTM

In this section, after introducing a method to swap configurations at adjacent replicas, we summarize the HMC algorithm on TLTM.

4.1. Swap of configurations at adjacent replicas

We realize the swap of configurations at adjacent replicas, Σ_{t_a} and Σ_{t_b} ($b = a \pm 1$), by the *exchange of the initial configurations*. Namely, $(z_a, z_b) \equiv (z_{t_a}(x), z_{t_b}(y)) \in \Sigma_{t_a} \times \Sigma_{t_b}$ is proposed to be updated to $(z'_a, z'_b) \equiv (z_{t_a}(x'), z_{t_b}(y')) \in \Sigma_{t_a} \times \Sigma_{t_b}$ with $(x', y') = (y, x)$ (see Fig. 4). Accordingly, the accept/reject probability must be with respect to $(x, y) \in \mathbb{R}^N \times \mathbb{R}^N$, and the algorithm takes the following form:

1. We first calculate the Jacobian matrices $J_a \equiv J_{t_a}(x)$, $J_b \equiv J_{t_b}(y)$.
2. We further calculate $z'_a \equiv z_{t_a}(y)$ and $z'_b \equiv z_{t_b}(x)$ together with the corresponding Jacobian matrices, $J'_a \equiv J_{t_a}(y)$ and $J'_b \equiv J_{t_b}(x)$.

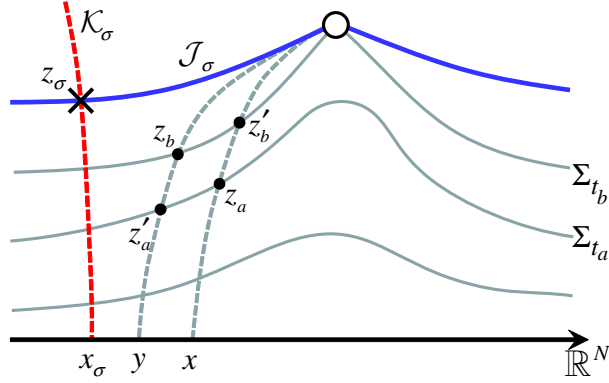


Figure 4: Swap of configurations from $(z_a, z_b) \equiv (z_{t_a}(x), z_{t_b}(y)) \in \Sigma_{t_a} \times \Sigma_{t_b}$ to $(z'_a, z'_b) \equiv (z_{t_a}(y), z_{t_b}(x)) \in \Sigma_{t_a} \times \Sigma_{t_b}$, which is actually the exchange of the initial configurations x and y . In figure, \mathcal{J}_σ is the Lefschetz thimble associated to a critical point z_σ . \mathcal{K}_σ is the corresponding anti-thimble. The distribution $\propto e^{-V(z)} = e^{-\text{Re } S(z)}$ on Σ_t has peaks at intersection points of Σ_t and \mathcal{K}_σ .

3. We update the original initial configurations (x, y) to the swapped initial configurations $(x', y') = (y, x)$ with the probability²⁴

$$\min \left(1, \frac{|\det J'_a| |\det J'_b| e^{-V(z'_a)-V(z'_b)}}{|\det J_a| |\det J_b| e^{-V(z_a)-V(z_b)}} \right). \quad (4.1)$$

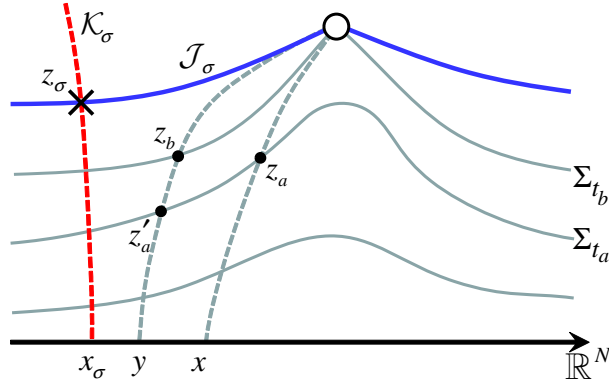


Figure 5: The case when $z_t(x)$ reaches a zero at $t < t_b$. We then simply reject the proposal for the swap $(x, y) \rightarrow (x', y') = (y, x)$.

The above procedure correctly leads to the global equilibrium on the product space $\Sigma_{\text{tot}} = \Sigma_{t_0} \times \cdots \times \Sigma_{t_A}$ with the distribution $p_{\text{eq}}(\vec{z}) \prod_{a=0}^A |dz_a| \propto \prod_{a=0}^A e^{-V(z_a)} |dz_a|$. In fact, by using the identity $|dz| = |\det J(x)| dx$, the transition probability $\hat{P}_{ab}^{(2)}(x', y'|x, y)$ from

²⁴For $z_a = z_{t_a}(x)$ and $z_b = z_{t_b}(y)$ with $t_a < t_b$, $z_t(x)$ may reach a zero at $t < t_b$ (see Fig. 5). In such a case, we reject the proposal for the swap $(x, y) \rightarrow (x', y') = (y, x)$. Note that this procedure keeps the relation (2.20).

$(x, y) \in \mathbb{R}^N \times \mathbb{R}^N$ to $(x', y') \in \mathbb{R}^N \times \mathbb{R}^N$ can be rewritten to the transition probability $P_{ab}^{(2)}(z'_a, z'_b | z_a, z_b)$ from $(z_a, z_b) = (z_{t_a}(x), z_{t_b}(y)) \in \Sigma_{t_a} \times \Sigma_{t_b}$ to $(z'_a, z'_b) = (z_{t_a}(x'), z_{t_b}(y')) \in \Sigma_{t_a} \times \Sigma_{t_b}$ as follows:

$$P_{ab}^{(2)}(z'_a, z'_b | z_a, z_b) = |\det J_{t_a}(x')|^{-1} |\det J_{t_b}(y')|^{-1} \hat{P}_{ab}^{(2)}(x', y' | x, y), \quad (4.2)$$

which means that the transition probability for $(x, y) \rightarrow (x', y')$ is translated to the following probability for $(z_a, z_b) \rightarrow (z'_a, z'_b)$:

$$P_{ab}^{(2)}(z'_a, z'_b | z_a, z_b) = \min \left(\frac{1}{|\det J'_a| |\det J'_b|}, \frac{e^{-V(z'_a)-V(z'_b)}}{|\det J_a| |\det J_b| e^{-V(z_a)-V(z_b)}} \right) \times \delta(x' - y) \delta(y' - x) \quad [(z'_a, z'_b) \neq (z_a, z_b)]. \quad (4.3)$$

Then one can easily show that the following detailed balance condition does hold:

$$P_{ab}^{(2)}(z'_a, z'_b | z_a, z_b) e^{-V(z_a)-V(z_b)} = P_{ab}^{(2)}(z_a, z_b | z'_a, z'_b) e^{-V(z'_a)-V(z'_b)}. \quad (4.4)$$

Note that we have to calculate the Jacobian determinant explicitly at every swapping process even though this is not mandatory for the molecular dynamics on each flowed surface.

We make an important comment on the reason why we use initial configurations as a reference in the swapping process. In general, one can introduce an arbitrary coordinate system to each flowed surface, to be used as a reference in swapping configurations as above. However, for such arbitrarily chosen coordinate systems, the distributions as functions of the coordinates will take very different functional forms between adjacent replicas, and one cannot expect a significant acceptance rate. On the other hand, this problem will not occur if we take the initial configurations as a common reference, because the distributions then have peaks at the same coordinate values (such as x_σ in Fig. 4 that flows to a critical point z_σ) for different flowed surfaces [12].

Another comment is that one can extend the molecular dynamics to the phase space of the whole enlarged configuration space, $T^*\Sigma_{t_0} \times \cdots \times T^*\Sigma_{t_A}$, also by swapping momenta π_a in the course of molecular dynamics, as in [30]. However, the additional computational cost will not be negligible, because in TLTM we need to transport $\pi_a \in T^*\Sigma_{t_a}$ (*resp.* $\pi_b \in T^*\Sigma_{t_b}$) to obtain $\pi'_b \in T^*\Sigma_{t_b}$ (*resp.* $\pi'_a \in T^*\Sigma_{t_a}$), and such a transport generically causes an additional difference in the sum of Hamiltonians, which lowers acceptance rates. We leave the investigation of this algorithm for future work.

4.2. Summary of HMC on TLTM

We summarize the HMC algorithm on the TLTM by following the outline given in subsection 2.3 (recall that $V(z) = \text{Re } S(z)$):

Step A. HMC on $\{\Sigma_{t_a}\}$:

Step A1 (initial setup). For a given configuration $\vec{z} = (z_a = z_{t_a}(x_a)) \in \Sigma_{\text{tot}} = \Sigma_{t_0} \times \dots \times \Sigma_{t_A}$, we generate $\vec{\pi} = (\tilde{\pi}_a) \in T_{z_0}^* \mathbb{R}^{2N} \times \dots \times T_{z_A}^* \mathbb{R}^{2N}$ with a Gaussian distribution $\propto \prod_a e^{-\tilde{\pi}_a^2/2M_a}$, and for every a we project $\tilde{\pi}_a \in T_{z_a}^* \mathbb{R}^{2N}$ to $\pi_a = \tilde{\pi}_a \mathcal{P}(z_a) \in T_{z_a}^* \Sigma_{t_a}$. The projection can be made with a direct method when the matrix elements of $J_a \equiv J_{t_a}(x_a)$ are known explicitly, or with an iterative method.

Step A2. For each $\zeta_a = (z_a, \pi_a) \in T^* \Sigma_{t_a}$ with $z_a = z_{t_a}(x_a)$, we find $w = (u, \lambda)^T$ that satisfies (3.30). The equation can be solved iteratively, $w_k \rightarrow w_{k+1} = w_k + \Delta w$, with Newton's method, starting from an initial guess $w_0 = (u_0, \lambda_0)^T$ and solving the linear equation (3.36) to obtain $\Delta w = (\Delta u, \Delta \lambda)^T$. Equation (3.36) can be solved with either of a direct method or an iterative method. After $w = (u, \lambda)^T$ is obtained, we set $x'_a = x_a + u$ and $z'_a = z_{t_a}(x'_a)$.

Step A3. For each replica a , we define

$$\pi_{a,1/2} \equiv \frac{1}{\Delta_S} M(z'_a - z_a), \quad (4.5)$$

and set

$$\tilde{\pi}'_a \equiv \pi_{a,1/2} - \frac{\Delta_S}{2} \partial \text{Re} S(z'_a). \quad (4.6)$$

Step A4. For each replica a , we project $\tilde{\pi}'_a \in T_{z'_a}^* \mathbb{R}^{2N}$ to $\pi'_a = \tilde{\pi}'_a \mathcal{P}(z'_a) \in T_{z'_a}^* \Sigma_{t_a}$. The projection can be made with a direct method when the matrix elements of $J'_a \equiv J_{t_a}(x'_a)$ are known explicitly, or with an iterative method.

Step A5. We repeat Steps A2 through A4 a fixed number of times ($\equiv n$) for all replicas.

Step A6. For each replica a , we calculate $\Delta H_a \equiv H_a(\zeta'_a) - H_a(\zeta_a)$, and update ζ_a to ζ'_a with the probability $\min(1, e^{-\Delta H_a})$.

Step A7. We ignore the values of π'_a and only keep those of z'_a .

Step B. Swap among $\{\Sigma_{t_a}\}$:

Step B1. For a given pair $(z_a, z_b) = (z_{t_a}(x), z_{t_b}(y)) \in \Sigma_{t_a} \times \Sigma_{t_b}$, we calculate the Jacobian matrices $J_a \equiv J_{t_a}(x)$, $J_b \equiv J_{t_b}(y)$ by numerically integrating the flow equations (2.9) and (3.28) if they have not been calculated yet.

Step B2. We calculate $z'_a \equiv z_{t_a}(y)$ and $z'_b \equiv z_{t_b}(x)$ together with the corresponding Jacobian matrices, $J'_a \equiv J_{t_a}(y)$ and $J'_b \equiv J_{t_b}(x)$.

Step B3. We update the original initial configurations (x, y) to the swapped initial configurations $(x', y') = (y, x)$ with the probability²⁵

$$\min \left(1, \frac{|\det J'_a| |\det J'_b| e^{-\text{Re } S(z'_a) - \text{Re } S(z'_b)}}{|\det J_a| |\det J_b| e^{-\text{Re } S(z_a) - \text{Re } S(z_b)}} \right). \quad (4.7)$$

Step C. Measurement:

After repeating Steps A and B sufficiently many times, we make a measurement and save the values $\{e^{i\theta(z_a)}, \mathcal{O}(z_a)\}$ ($a = 0, \dots, A$), that are calculated from z_a and J_a .

5. Results and analysis

In this section, we apply the TLTM to the Hubbard model both with HMC (implemented in this paper) and with Metropolis (adopted in [11, 12]). We first confirm both algorithms to work properly by showing that the expectation value of the number density operator is estimated correctly. We then show that HMC is more efficient than Metropolis even for small degrees of freedom ($N = 20$).

5.1. Hubbard model and the parameters for simulations

Let Λ be a lattice with N_s sites. The Hubbard model on Λ is defined by the Hamiltonian

$$\begin{aligned} H = & -\kappa \sum_{\mathbf{x}, \mathbf{y}} \sum_{\sigma} K_{\mathbf{xy}} c_{\mathbf{x}, \sigma}^{\dagger} c_{\mathbf{y}, \sigma} - \mu \sum_{\mathbf{x}} (n_{\mathbf{x}, \uparrow} + n_{\mathbf{x}, \downarrow} - 1) \\ & + U \sum_{\mathbf{x}} (n_{\mathbf{x}, \uparrow} - 1/2) (n_{\mathbf{x}, \downarrow} - 1/2). \end{aligned} \quad (5.1)$$

Here, $c_{\mathbf{x}, \sigma}$ and $c_{\mathbf{x}, \sigma}^{\dagger}$ are the annihilation and creation operators on site $\mathbf{x} \in \Lambda$ with spin σ ($=\uparrow, \downarrow$), obeying $\{c_{\mathbf{x}, \sigma}, c_{\mathbf{y}, \tau}^{\dagger}\} = \delta_{\mathbf{xy}} \delta_{\sigma\tau}$ and $\{c_{\mathbf{x}, \sigma}, c_{\mathbf{y}, \tau}\} = \{c_{\mathbf{x}, \sigma}^{\dagger}, c_{\mathbf{y}, \tau}^{\dagger}\} = 0$, and $n_{\mathbf{x}, \sigma} \equiv c_{\mathbf{x}, \sigma}^{\dagger} c_{\mathbf{x}, \sigma}$. $K_{\mathbf{xy}}$ is the adjacency matrix that takes a nonvanishing value ($\equiv 1$) only for nearest neighbors, and we assume the lattice to be bipartite. $\kappa (> 0)$ is the hopping parameter, μ is the chemical potential, and $U (> 0)$ represents the strength of the on-site repulsive potential. We have shifted $n_{\mathbf{x}, \sigma}$ as $n_{\mathbf{x}, \sigma} - 1/2$ so that $\mu = 0$ corresponds to the half-filling state, $\sum_{\sigma} \langle n_{\mathbf{x}, \sigma} - 1/2 \rangle = 0$.

By using the Trotter decomposition with equal spacing ϵ ($\beta = N_{\tau}\epsilon$), we can rewrite the expectation value of the number density $n \equiv (1/N_s) \sum_{\mathbf{x}} (n_{\mathbf{x}, \uparrow} + n_{\mathbf{x}, \downarrow} - 1)$ as a path integral over a Gaussian Hubbard-Stratonovich variable $\phi = (\phi_{\ell, \mathbf{x}})$ as follows (see, e.g., [12] for the

²⁵See a notice in footnote 24.

derivation):

$$\langle n \rangle \equiv \frac{\int d\phi e^{-S(\phi)} n(\phi)}{\int d\phi e^{-S(\phi)}} \quad \left(d\phi \equiv \prod_{\ell, \mathbf{x}} d\phi_{\ell, \mathbf{x}} \right), \quad (5.2)$$

$$e^{-S(\phi)} \equiv e^{-(1/2) \sum_{\ell, \mathbf{x}} \phi_{\ell, \mathbf{x}}^2} \det M^a(\phi) \det M^b(\phi), \quad (5.3)$$

$$M^{a/b}(\phi) \equiv \mathbf{1} + e^{\pm \beta \mu} \prod_{\ell} e^{\epsilon \kappa K} e^{\pm i \sqrt{\epsilon U} \phi_{\ell}}, \quad (5.4)$$

$$n(\phi) \equiv (i \sqrt{\epsilon U} N_{\tau} N_s)^{-1} \sum_{\ell, \mathbf{x}} \phi_{\ell, \mathbf{x}}, \quad (5.5)$$

where $\phi_{\ell} \equiv (\phi_{\ell, \mathbf{x}} \delta_{\mathbf{x}\mathbf{y}})$ and \prod_{ℓ} is a product in descending order. Below we apply the TLTM to this model, in which the variables $\phi = (\phi_{l, \mathbf{x}})$ correspond to $x = (x^i)$ with $i = 1, \dots, N (\equiv N_{\tau} N_s)$.

We use a two-dimensional periodic square lattice of size 2×2 (thus $N_s = 4$). The parameters in the Hamiltonian are set to $\beta \kappa = 3$, $\beta \mu = 4$, $\beta U = 13$. The imaginary time is decomposed to $N_{\tau} = 5$ pieces. We set $A = 6$, $T = 0.24$ (maximum flow time), and t_a 's are set linearly in a .²⁶ We use as an initial configuration the one obtained after a test run. The same initial configuration is used for HMC and Metropolis. After discarding 2,000 configurations to ensure equilibration, we take $N_{\text{conf}} = 30,000$ configurations for estimations. In both algorithms, we first perform swapping process, then make transitions on each flowed surface, and finally make measurements.

In molecular dynamics, we set the step size to $\Delta s = 0.1$ and the step number to $n = 10$. We set $\sigma_a^2 = 1$ in $(M_a)_{IJ} = \sigma_a^2 \delta_{IJ}$ for all a , and use the direct methods for the inversions in Steps A1, A2 and A4 in subsection 4.2.²⁷ In solving (3.36) iteratively, we set the initial guess to $w_0 = 0$, and rescale Δw as $\Delta w \rightarrow 0.15 \times \Delta w$ when $|\Delta w|/\sqrt{2N}$ is larger than $0.5 \times \Delta s / |\det J_{t_a}(x)|^{1/N}$ or when $|f(w_k + \Delta w)| > |f(w_k)|$ (see appendix A for a detailed explanation on the conditions for the scaling). We set the stopping criterion to $|\Delta w|/\sqrt{2N} < 10^{-8}$ and $|f(w_k)|/\sqrt{2N} < 10^{-5}$. We find that the process terminates with 3–7 iterations in most cases. The momentum is flipped either when the number of iterations exceeds 50 or when $x + u_k + \Delta u$ still flows to a zero of $e^{-S(z)}$ even after the rescaling $\Delta w \rightarrow 0.15^3 \times \Delta w$ (see also appendix A on the condition for the replacement). We have tested the reversibility for some configurations chosen in the vicinity of zeros of $e^{-S(z)}$, and found that $|z' - z|/\sqrt{2N}$ is around $O(10^{-10})$ for $(z', \pi') = (\Phi_{\Delta s}^{n=10} \circ \Psi \circ \Phi_{\Delta s}^{10})(z, \pi)$ where π is generated from a Gaussian distribution with unit variance.

For Metropolis, we use the isotropic Gaussian proposals of the standard deviations $\sigma_{\text{Met}} = 0.037 - 0.18$ (varying on replicas), which are tuned so that the acceptance rate is 0.5–0.7

²⁶See [12] for a justification of the linear spacing that is based on the geometrical optimization [31, 32].

²⁷The direct method (LU decomposition) turns out to be faster than the iterative method (BiCGStab) for the case we consider with small degrees of freedom.

(see Table 1). We repeat this procedure $n_{\text{Met}} = 50$ times.

The swapping process is performed by pairing seven replicas in two different ways. One is (i): $(a, b) = (0, 1), (2, 3), (4, 5)$ leaving replica 6 intact, and the other is (ii): $(1, 2), (3, 4), (5, 6)$ leaving replica 0 intact. We repeat the swap seven times changing the pairing (i) and (ii) alternately.²⁸ The acceptance rates thus obtained are shown in Table 2.²⁹

algorithm	parameter	$a = 0$	1	2	3	4	5	6
HMC	Δs	0.1	0.1	0.1	0.1	0.1	0.1	0.1
	n	10	10	10	10	10	10	10
Metropolis	σ_{Met}	0.18	0.13	0.10	0.081	0.066	0.038	0.037
	n_{Met}	50	50	50	50	50	50	50

Table 1: The parameters in HMC and Metropolis.

algorithm	direction	$a = 0$	1	2	3	4	5	6
HMC (w/ swap)	x (or z)	0.99	0.98	0.96	0.95	0.94	0.94	0.94
	a	0.52	0.48	0.47	0.46	0.46	0.45	-
Metropolis (w/ swap)	x (or z)	0.53	0.54	0.55	0.55	0.55	0.66	0.61
	a	0.52	0.48	0.47	0.46	0.46	0.45	-
HMC (w/o swap)	x (or z)	0.99	0.98	0.96	0.95	0.94	0.91	0.96
Metropolis (w/o swap)	x (or z)	0.53	0.54	0.55	0.55	0.55	0.57	0.67

Table 2: The average acceptance rates.

Calculations without swap are also carried out for comparison, with the same parameters and the same initial configuration as those for the calculations with swap.

5.2. Estimate of the number density

In order to confirm the algorithms to work correctly, we evaluate the expectation values of the number density, $\langle n \rangle$. The sign averages and the expectation values are shown in Figs. 6 and 7. We fit the data points in the range $a = 3, \dots, 6$ for both HMC and Metropolis, which are chosen by observing that $|\overline{e^{i\theta(z_a)}}|$ are above $3/\sqrt{2N_{\text{conf}}}$ including the error margin [12]. The results are $\langle n \rangle \approx 0.1145 \pm 0.0076$ for HMC ($\chi^2/\text{DOF} = 0.48$), and $\langle n \rangle \approx 0.120 \pm 0.011$ for Metropolis ($\chi^2/\text{DOF} = 0.44$), that should be compared with the exact value $\langle n \rangle = 0.1143$

²⁸By making independent pairs of replicas in this way, the swap can be performed in parallel processes.

²⁹The acceptance rates for HMC may seem too large. They can actually be reduced by increasing Δs , but this must be done carefully, because for too large Δs Newton's method in solving (3.32) may converge to unwanted solutions, which violates the reversibility (see discussions in appendix A).

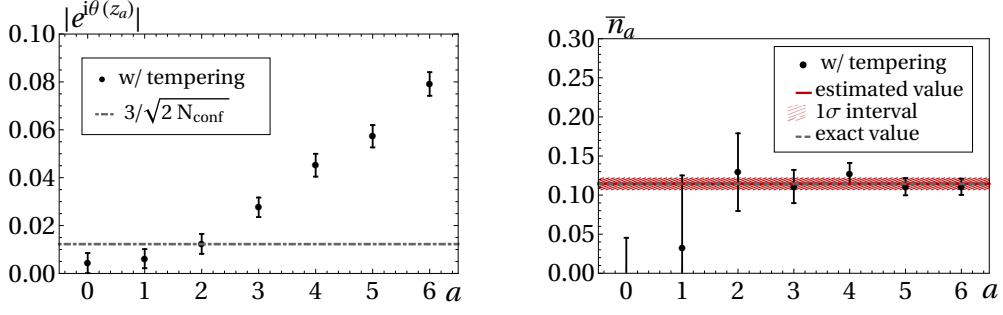


Figure 6: The results for HMC with swap. (Left) The sign averages. (Right) The estimates \bar{n}_a .

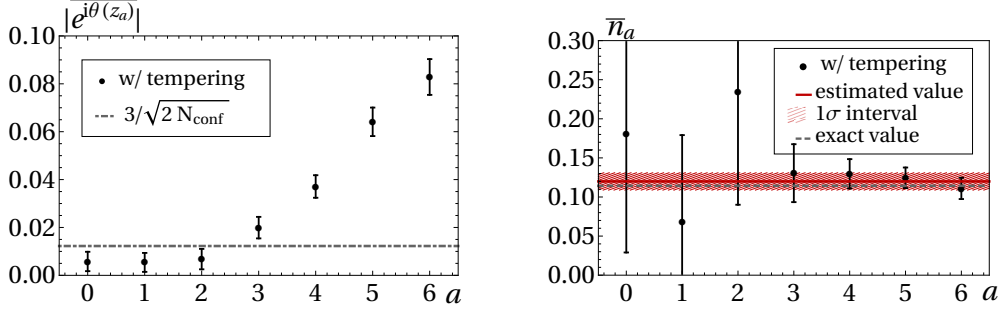


Figure 7: The results for Metropolis with swap. (Left) The sign averages. (Right) The estimates \bar{n}_a .

(the value under the Trotter decomposition [12]), and thus we confirm that the algorithms work correctly.

We also plot the sign averages and the expectation values obtained *without* swap in Figs. 8 and 9. For large t , we observe significant deviations from the exact value but small

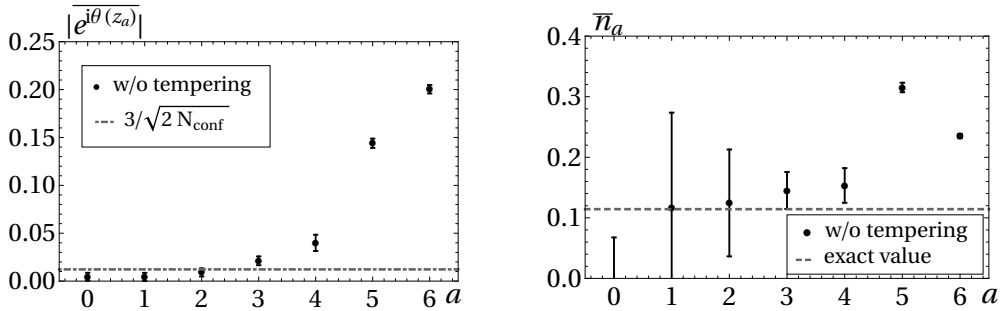


Figure 8: The results for HMC without swap. (Left) The sign averages. (Right) The estimates \bar{n}_a .

error margins, reflecting the presence of the ergodicity problem [12].

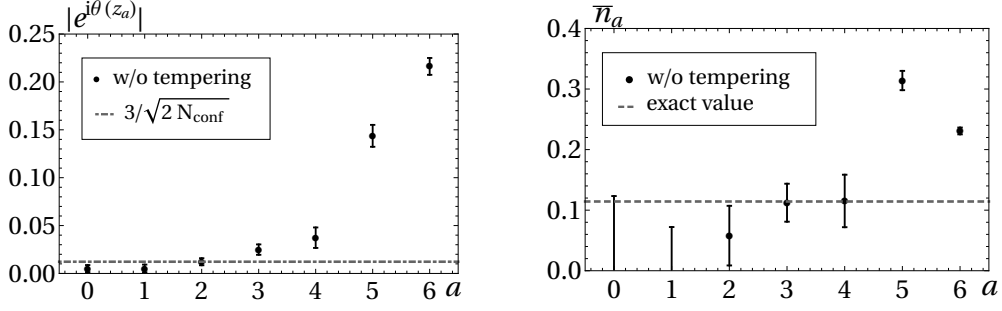


Figure 9: The results for Metropolis without swap. (Left) The sign averages. (Right) The estimates \bar{n}_a .

5.3. Autocorrelations

In this subsection, we evaluate the autocorrelations for both HMC and Metropolis, and compare their efficiencies. For the evaluation, we estimate the normalized autocorrelation function by (see, e.g., [33, 34])

$$\rho(m) = \frac{C(m)}{C(0)}. \quad (5.6)$$

Here, $C(m)$ is given by

$$C(m) \equiv \frac{1}{N_{\text{conf}} - m} \sum_{k=1}^{N_{\text{conf}} - m} [f(z_a^{(k)}) - \overline{f(z_a)}][f(z_a^{(k+m)}) - \overline{f(z_a)}], \quad (5.7)$$

where $\overline{f(z_a)}$ is a sample average for the subsample at replica a , $\overline{f(z_a)} \equiv (1/N_{\text{conf}}) \sum_{k=1}^{N_{\text{conf}}} f(z_a^{(k)})$ (see subsection 2.1). Then, we estimate the integrated autocorrelation time by the following formula, which is valid for $\tau_{\text{int}} \ll k_{\text{max}} \ll N_{\text{conf}}$ [34]:

$$\tau_{\text{int}} = 1 + 2 \sum_{k=1}^{k_{\text{max}}} \rho(k). \quad (5.8)$$

When we plot the right-hand side of eq. (5.8) as a function of k_{max} , we expect to observe a plateau. In the following, we choose the plateau region manually, and define the estimate of τ_{int} to be the value of τ_{int} at the least k_{max} in the region. Note that $\rho(m)$ and τ_{int} depend on the choice of operators and replicas. We apply the above formulas to the operators $f(z) = \text{Re}[e^{i\theta(z)}n(z)]$ and $f(z) = \text{Re}[e^{i\theta(z)}] = \cos\theta(z)$ at replica $a = A$.

We first investigate the autocorrelation for $f(z) = \text{Re}[e^{i\theta(z)}n(z)]$. Figure 10 shows τ_{int} for various k_{max} , from which we identify the plateau and estimate τ_{int} as given in Table 3. We see that τ_{int} for HMC is about 50% of that for Metropolis with respect to this operator. A similar analysis is carried out for $f(z) = \cos\theta(z)$ (see Fig. 11). The estimates of τ_{int} are also given in Table 3. We see that τ_{int} for HMC is also about 50% of that for Metropolis with respect to this operator.

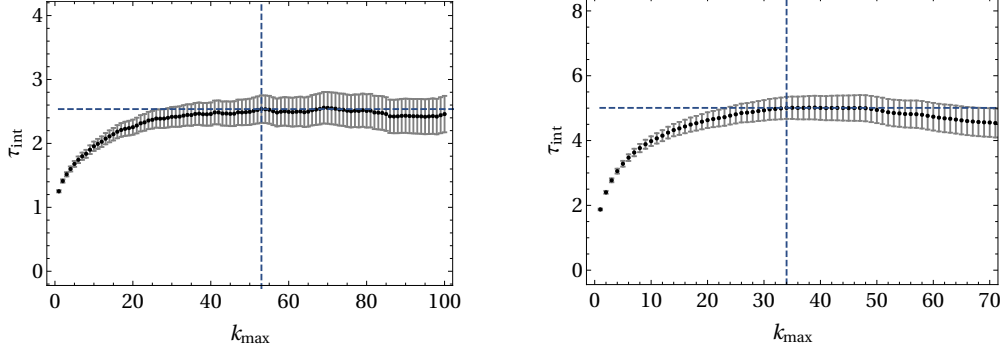


Figure 10: The estimates of τ_{int} for $\text{Re}[e^{i\theta(z)}n(z)]$ (with swap). (Left) HMC. (Right) Metropolis. The horizontal dashed line indicates the value of τ_{int} , and the vertical dashed line indicates the value of k_{max} ,

$f(z)$	algorithm	τ_{int}	k_{max}
$\text{Re}[e^{i\theta(z)}n(z)]$	HMC	2.54 ± 0.21	53
	Metropolis	5.01 ± 0.34	34
$\cos \theta(z)$	HMC	1.630 ± 0.093	24
	Metropolis	3.53 ± 0.23	30

Table 3: The estimates of τ_{int} (with swap).

As a comparison of the actual efficiency between the two algorithms, we comment that the elapsed time to obtain a single configuration is in average 7.8 sec for HMC and 15 sec for Metropolis.³⁰ Therefore, the actual computational cost to obtain one independent configuration with HMC is about 30% of that with Metropolis. We expect that the benefits in computational cost become more significant as the degrees of freedom increase.

We here comment that the difference of τ_{int} between HMC and Metropolis becomes more significant for simulations *without* swap. In Table 4 we summarize the results obtained without swap. The corresponding plots for $f(z) = \text{Re}[e^{i\theta(z)}n(z)]$ are shown in Fig. 12, and

$f(z)$	algorithm	τ_{int}	k_{max}
$\text{Re}[e^{i\theta(z)}n(z)]$	HMC	1.529 ± 0.048	7
	Metropolis	11.5 ± 1.0	57
$\cos \theta(z)$	HMC	1.340 ± 0.033	4
	Metropolis	5.16 ± 0.38	41

Table 4: The estimates of τ_{int} (without swap).

those for $f(z) = \cos \theta(z)$ in Fig. 13. We see that τ_{int} for HMC is 13 – 26% of those for

³⁰The estimations were made by using Intel Xeon E5-2667 v4 running at 3.2 GHz with seven threads for each algorithm.

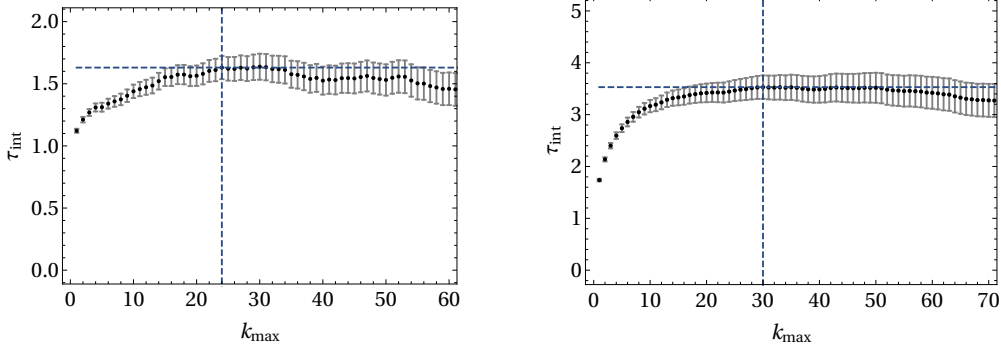


Figure 11: The estimates of τ_{int} for $\cos \theta(z)$ (with swap). (Left) HMC. (Right) Metropolis.

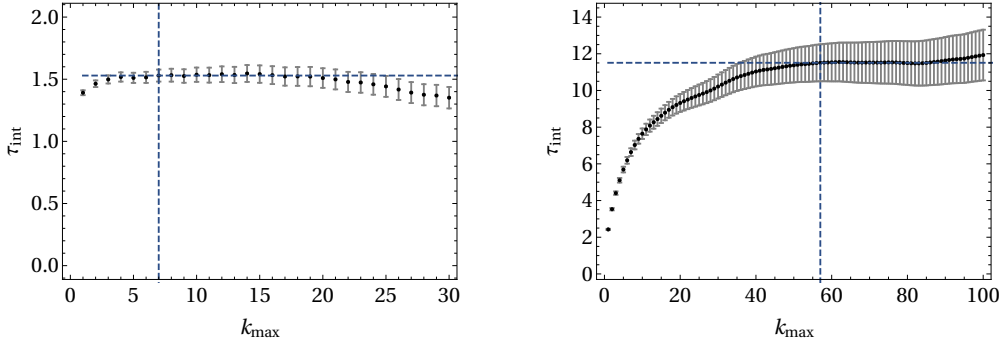


Figure 12: The estimates of τ_{int} for $\text{Re}[e^{i\theta(z)}n(z)]$ (without swap). (Left) HMC. (Right) Metropolis.

Metropolis . The elapsed time to obtain a single configuration is in average 4.1 sec for HMC and 12 sec for Metropolis.³¹ Thus the actual computational cost to obtain one independent configuration with HMC is less than 10% of that with Metropolis for the calculations without swap.

6. Conclusion and outlook

In this paper, we implemented the HMC algorithm on the TLTM, aiming to apply our algorithm to systems including fermions with large degrees of freedom. We observed that the actual computational cost to obtain an independent configuration becomes about 30% of that for the Metropolis algorithm even for such small degrees of freedom ($N = 20$).

We expect that the above improvement makes the TLTM more effective in solving the sign problems listed in Introduction, especially when performed on a large-scale computer. In parallel with the application of the algorithm to those problems (and also to some simplified model such as chiral random matrix models [35, 36]), it should be important to further

³¹The estimations were made with the same environment as footnote 30.

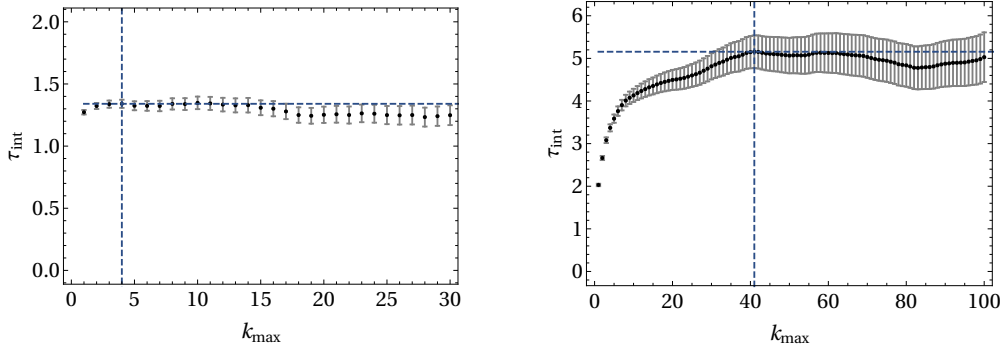


Figure 13: The estimates of τ_{int} for $\cos \theta(z)$ (without swap). (Left) HMC. (Right) Metropolis.

develop the algorithm itself. In particular, the following three issues should be addressed:

(1) It is desirable to have a systematic method to estimate numerical errors introduced in integrating the antiholomorphic gradient flow and in solving Newton's method iteratively (Step 1 in subsection 3.2).

(2) We should investigate the scaling of computational cost as the degrees of freedom are increased. A simple estimate of the total cost of our algorithm is $O(N^{3-4})$. $O(N^3)$ comes from the calculation of the Jacobian, and $O(N^{0-1})$ comes from the need to increase the number of replicas to keep the acceptance rates at swapping to significant values. It should be crucial to investigate if the above scaling is actually realized in large-scale calculations, because it then means that we can obtain correct results with a computational cost of a power of N (not an exponential of N).

(3) It should be helpful to have a systematic understanding of the global sign problem (i.e. cancellations of phases among different thimbles) and the residual sign problem (i.e. contributions from the phase factor $e^{i\varphi(z)}$) for systems with large degrees of freedom, because they can be a cause of a significant increase of computational cost.

A study along these lines is now in progress and will be reported elsewhere.

Acknowledgments

The authors thank Andrei Alexandru, Gerald Dunne, Hitotsugu Fujii, Yoshimasa Hidaka, Ken-Ichi Ishikawa, Issaku Kanamori, Masakiyo Kitazawa, Yoshifumi Nakamura, Yusuke Namekawa, Jun Nishimura, Akira Ohnishi, Yusuke Taniguchi and Shoichiro Tsusui for useful discussions, and especially Yoshio Kikukawa for sharing his insights on the RATTLE process in Lefschetz thimble methods. This work was partially supported by JSPS KAKENHI (Grant Numbers 16K05321, 18J22698 and 17J08709) and by SPIRITS 2019 of Kyoto University (PI: M.F.).

A. More on the treatment of zeros

In subsection 3.2, we constructed a molecular dynamics on Σ_t , where a point $z = z_t(x)$ moves to another point $z' = z_t(x + u)$, and the increment $u = (u^\alpha) \in \mathbb{R}^N$ is obtained by solving (3.30) with respect to $w = (u^\alpha, \lambda^\alpha)^T \in \mathbb{R}^{2N}$.

Among possible solutions for $w = (u, \lambda)^T$, we look for the solution that gives $z' = z_t(x + u)$ closest to z , which will ensure the molecular-dynamics step to satisfy the reversibility. Since $u = O(\Delta s)$ and $\lambda = O(\Delta s^2)$ (Δs : step size of molecular dynamics), we would expect that such solution can be found uniquely by setting Δs to a sufficiently small value and by iteratively solving (3.30) with Newton's method, $w_k \rightarrow w_{k+1} = w_k + \Delta w$ [see (3.36)], with the initial guess $w_0 = 0$. However, special attention needs to be paid when $z = z_t(x)$ is near a zero of the weight $e^{-S(z)}$, because this means that the initial configuration x is close to a domain D_t that consists of the points flowing to the zero with flow times less than t (see Fig. 14). Then, there can be a solution that gives $x + u$ in a region beyond D_t (see the right panel of Fig. 14). However, this solution is not what we are looking for because this can give u much larger than $O(\Delta s)$. Such a case can be identified if we observe that the sequence

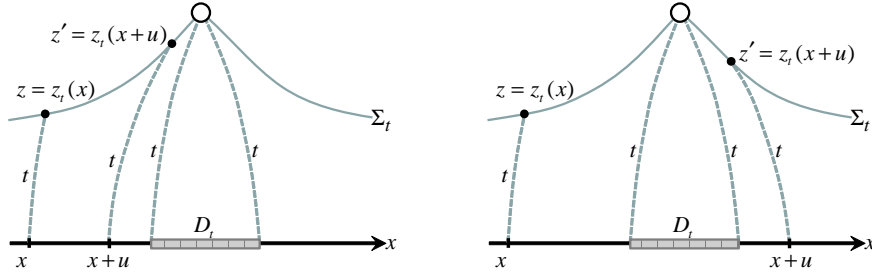


Figure 14: Possible solutions to (3.30). D_t is the domain consisting of the points that flow to a zero (denoted by a circle) with flow times less than t . $x + u$ is on the same side as x (left), or in a region beyond D_t (right).

$x + u_k + \Delta u$ enters the domain D_t while keeping the increment Δw (and thus Δu) to small values so that the sequence does not leap over D_t (see Fig. 15). Note that there can also be a case where a solution is not found anywhere.

The above consideration leads us to the following algorithm:

Step 1. We start from the initial guess $w_0 = 0$, and at every step $w_k \rightarrow w_{k+1} = w_k + \Delta w$, we rescale the obtained Δw as $\Delta w \rightarrow 0.15 \times \Delta w$ unless $|\Delta w|/\sqrt{2N} < 0.5 \times \Delta s/|\det J_t(x)|^{1/N}$ and $|f(w_k + \Delta w)| < |f(w_k)|$.³²

³²The requirement with the first inequality is that the “typical magnitude” of w^I ($I = 1, \dots, 2N$) (which we estimate to be $|w|/\sqrt{2N}$) be less than $0.5 \Delta s$ even after it is stretched under the flow (by a factor which we estimate to be $|\det J_t(x)|^{1/N}$). The second inequality prohibits the sequence to go away from a nearby solution.

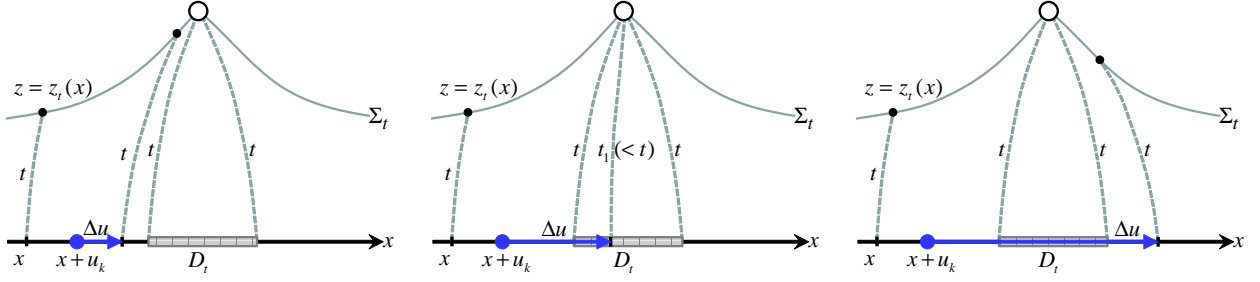


Figure 15: An iterative step in Newton's method giving $u_{k+1} = u_k + \Delta u$. $x + u_{k+1}$ can be on the same side as x (left), in the domain D_t (middle), or in a region beyond D_t (right).

Step 2. We continue the iterative steps until we reach one of the following three cases:

- (A) The sequence converges to a solution.
- (B) The sequence enters the domain D_t .
- (C) The sequence will not converge to any solution.

As a criterion for (A), we use the conditions $|\Delta w|/\sqrt{2N} < 10^{-8}$ and $|f(w_k)|/\sqrt{2N} < 10^{-5}$. Case (B) is identified if $x + u_k + \Delta u$, at some step k , flows to a zero with a flow time less than t even after the rescaling $\Delta w \rightarrow 0.15^3 \times \Delta w$. Case (C) is identified if the number of iterations exceeds 50. As a comparison, we find that the process terminates with 3 – 7 iterations for case (A).

Step 3. For case (A), we set $z' \equiv z_t(x + u) \in \Sigma_t$ and calculate $\pi' \in T^*\Sigma_t$ to get $(z', \pi') = \Phi_{\Delta s}(z, \pi)$. For cases (B) and (C), we stop the iteration and set $(z', \pi') \equiv (z, -\pi) (= \Psi(z, \pi))$, i.e., we use the momentum flip Ψ instead of $\Phi_{\Delta s}$.

References

- [1] G. Aarts, “Introductory lectures on lattice QCD at nonzero baryon number,” J. Phys. Conf. Ser. **706**, no. 2, 022004 (2016) [arXiv:1512.05145 [hep-lat]].
- [2] J. E. Hirsch, “Two-dimensional Hubbard model: Numerical simulation study,” Phys. Rev. B **31**, 4403 (1985).
- [3] E. Y. Loh, J. E. Gubernatis, R. T. Scalettar, S. R. White, D. J. Scalapino and R. L. Sugar, “Sign problem in the numerical simulation of many-electron systems,” Phys. Rev. B **41**, 9301 (1990).
- [4] M. Cristoforetti, F. Di Renzo and L. Scorzato, “New approach to the sign problem in quantum field theories: High density QCD on a Lefschetz thimble,” Phys. Rev. D **86**, 074506 (2012) [arXiv:1205.3996 [hep-lat]].

- [5] M. Cristoforetti, F. Di Renzo, A. Mukherjee and L. Scorzato, “Monte Carlo simulations on the Lefschetz thimble: Taming the sign problem,” *Phys. Rev. D* **88**, no. 5, 051501(R) (2013) [arXiv:1303.7204 [hep-lat]].
- [6] A. Mukherjee, M. Cristoforetti and L. Scorzato, “Metropolis Monte Carlo integration on the Lefschetz thimble: Application to a one-plaquette model,” *Phys. Rev. D* **88**, no. 5, 051502(R) (2013) [arXiv:1308.0233 [physics.comp-ph]].
- [7] H. Fujii, D. Honda, M. Kato, Y. Kikukawa, S. Komatsu and T. Sano, “Hybrid Monte Carlo on Lefschetz thimbles - A study of the residual sign problem,” *JHEP* **1310**, 147 (2013) [arXiv:1309.4371 [hep-lat]].
- [8] M. Cristoforetti, F. Di Renzo, G. Eruzzi, A. Mukherjee, C. Schmidt, L. Scorzato and C. Torrero, “An efficient method to compute the residual phase on a Lefschetz thimble,” *Phys. Rev. D* **89**, no. 11, 114505 (2014) [arXiv:1403.5637 [hep-lat]].
- [9] A. Alexandru, G. Başar and P. Bedaque, “Monte Carlo algorithm for simulating fermions on Lefschetz thimbles,” *Phys. Rev. D* **93**, no. 1, 014504 (2016) [arXiv:1510.03258 [hep-lat]].
- [10] A. Alexandru, G. Başar, P. F. Bedaque, G. W. Ridgway and N. C. Warrington, “Sign problem and Monte Carlo calculations beyond Lefschetz thimbles,” *JHEP* **1605**, 053 (2016) [arXiv:1512.08764 [hep-lat]].
- [11] M. Fukuma and N. Umeda, “Parallel tempering algorithm for integration over Lefschetz thimbles,” *PTEP* **2017**, no. 7, 073B01 (2017) [arXiv:1703.00861 [hep-lat]].
- [12] M. Fukuma, N. Matsumoto and N. Umeda, “Applying the tempered Lefschetz thimble method to the Hubbard model away from half filling,” *Phys. Rev. D* **100**, no. 11, 114510 (2019) [arXiv:1906.04243 [cond-mat.str-el]].
- [13] E. Witten, “Analytic continuation of Chern-Simons theory,” *AMS/IP Stud. Adv. Math.* **50**, 347 (2011) [arXiv:1001.2933 [hep-th]].
- [14] A. Alexandru, G. Başar, P. F. Bedaque and N. C. Warrington, “Tempered transitions between thimbles,” *Phys. Rev. D* **96**, no. 3, 034513 (2017) [arXiv:1703.02414 [hep-lat]].
- [15] S. Duane, A. D. Kennedy, B. J. Pendleton and D. Roweth, “Hybrid Monte Carlo,” *Phys. Lett. B* **195**, 216 (1987).
- [16] M. Creutz, “Global Monte Carlo algorithms for many-fermion systems,” *Phys. Rev. D* **38**, 1228 (1988).
- [17] H. C. Andersen, “RATTLE: A “velocity” version of the SHAKE algorithm for molecular dynamics calculations,” *J. Comput. Phys.* **52**, 24 (1983).
- [18] B. J. Leimkuhler and R. D. Skeel, “Symplectic numerical integrators in constrained Hamiltonian systems,” *J. Comput. Phys.* **112**, 117 (1994).

- [19] A. Alexandru, “Improved algorithms for generalized thimble method,” talk at the 37th international conference on lattice field theory, Wuhan, 2019.
- [20] A. Mukherjee and M. Cristoforetti, “Lefschetz thimble Monte Carlo for many-body theories: A Hubbard model study,” *Phys. Rev. B* **90**, no. 3, 035134 (2014) [arXiv:1403.5680 [cond-mat.str-el]].
- [21] Y. Tanizaki, Y. Hidaka and T. Hayata, “Lefschetz-thimble analysis of the sign problem in one-site fermion model,” *New J. Phys.* **18**, no. 3, 033002 (2016) [arXiv:1509.07146 [hep-th]].
- [22] M. Ulybyshev, C. Winterowd and S. Zafeiropoulos, “Taming the sign problem of the finite density Hubbard model via Lefschetz thimbles,” [arXiv:1906.02726 [cond-mat.str-el]].
- [23] M. Ulybyshev, C. Winterowd and S. Zafeiropoulos, “Lefschetz thimbles decomposition for the Hubbard model on the hexagonal lattice,” [arXiv:1906.07678 [cond-mat.str-el]].
- [24] R. H. Swendsen and J.-S. Wang, “Replica Monte Carlo Simulation of Spin-Glasses,” *Phys. Rev. Lett.* **57**, 2607 (1986).
- [25] C. J. Geyer, “Markov Chain Monte Carlo Maximum Likelihood,” in *Computing Science and Statistics: Proceedings of the 23rd Symposium on the Interface*, American Statistical Association, New York, p. 156 (1991).
- [26] K. Hukushima and K. Nemoto, “Exchange Monte Carlo method and application to spin glass simulations,” *J. Phys. Soc. Jpn.* **65**, 1604 (1996).
- [27] Y. Saad and M. H. Schultz, “GMRES: A Generalized minimal residual algorithm for solving nonsymmetric linear systems,” *SIAM J. Sci. and Stat. Comput.* **7**, 856 (1986).
- [28] H. A. van der Vorst, “Bi-CGSTAB: A fast and smoothly converging variant of Bi-CG for the solution of nonsymmetric linear systems,” *SIAM J. Sci. and Stat. Comput.* **13**, 631 (1992).
- [29] A. Alexandru, G. Basar, P. F. Bedaque and G. W. Ridgway, “Schwinger-Keldysh formalism on the lattice: A faster algorithm and its application to field theory,” *Phys. Rev. D* **95**, no. 11, 114501 (2017) [arXiv:1704.06404 [hep-lat]].
- [30] Y. Sugita and Y. Okamoto, “Replica-exchange molecular dynamics method for protein folding,” *Chem. Phys. Lett.* **314**, 141 (1999).
- [31] M. Fukuma, N. Matsumoto and N. Umeda, “Distance between configurations in Markov chain Monte Carlo simulations,” *JHEP* **1712**, 001 (2017) [arXiv:1705.06097 [hep-lat]].
- [32] M. Fukuma, N. Matsumoto and N. Umeda, “Emergence of AdS geometry in the simulated tempering algorithm,” *JHEP* **1811**, 060 (2018) [arXiv:1806.10915 [hep-th]].

- [33] M. B. Priestley, “Spectral analysis and time series,” Academic Press, London (1981).
- [34] N. Madras and A. D. Sokal, “The pivot algorithm: A highly efficient Monte Carlo method for self-avoiding walk,” *J. Stat. Phys.* **50**, 109 (1988).
- [35] M. A. Stephanov, “Random matrix model of QCD at finite density and the nature of the quenched limit,” *Phys. Rev. Lett.* **76**, 4472 (1996) [hep-lat/9604003].
- [36] M. A. Halasz, A. D. Jackson, R. E. Shrock, M. A. Stephanov and J. J. M. Verbaarschot, “On the phase diagram of QCD,” *Phys. Rev. D* **58**, 096007 (1998) [hep-ph/9804290].